Multimedia Tools and Applications (2019) 78:14443–14463
https://doi.org/10.1007/s11042-018-6623-z

Similarity estimation based on sparse spectral correspondence

Li Han[1] · Dan Li[1] · Shu Ning Liu[1] · Yu Nan Liu[1] · Di Tang[1]

Received: 12 June 2017 / Revised: 22 March 2018 / Accepted: 27 August 2018 /
Published online: 7 November 2018

Abstract
We present a sparse spectral correspondence method for deformable shape analysis. Our method exploits randomized sampling for sparse shape representation. By choosing a random subset of points that preserve key properties of the entire data set, it allows one to run algorithms efficiently on a small sample. First we implement random row sampling of an undirected weighted graph matrix by "Lewis weights", which can be viewed as statistical leverage scores of a reweighted matrix and used directly as sampling probabilities. Second, a sparse graph is constructed on selected sample points by using minimum spanning tree (MST). We then discover the meaningful structural correspondence based on TPS (thin-plate spline) approach in the spectral embedded space. Finally we show how we use the sparse spectral correspondence to implement similarity estimation for shape matching and classification for different topological shapes. A series of experimental results demonstrate that our method is accurate and robust for shape analysis.

Keywords Shape analysis · Shape correspondence · Spectral eigenmap · Non-rigid shape · Sparse representation

1 Introduction

Shape analysis has been an extensively studied research topic in Computer Graphics and Computer Vision. One particular task is to provide similarity measurement among shapes, that can be effectively used for shape understanding, shape matching, shape retrieval, shape editing and reconstruction, etc.

Most methods have focused on how to find geometric criteria for extracting shape descriptors. Such approaches are limited to a single generic rule (e.g., concavity, skeleton topology, approximate shape primitives) or a single feature (area, angular distance, shape diameter, curvature tensor, and geodesic distance) to partition the input mesh. However, they usually lack efficiency and consistency for complex deformable shape matching.

✉ Li Han
hl_dlls@dl.cn

[1] School of Computer and Information Technology, Liaoning Normal University, Dalian, China

Our method combines sparse sampling method with spectral correspondence for efficient and intrinsic shape analysis. For a set of 3D shapes from different categories as input, we first extract a set of sample points to build a sparse representation for each shape by using an efficient row sampling method, and then the affinity matrix is created based on minimum spanning tree. We embed the set of weighted matrices into spectral domain to find the intrinsic structural correspondence and build the pairwise matching matrix between each two meshes. After that, we combine all single weighted matrices and pair-wise matching matrices to reveal the structural consistency for the input set.

We have tested the proposed approach on various categories of shapes. The final results demonstrate that our approach is efficient for shape classification despite the considerable changes of their topology, stretching and pose-variances and incompleteness.

The paper is structured as follows: the related works are presented in Section 2. Section 3 details the extraction of sampling points, the construction of sparse graph and the transformation from spatial domain into spectral domain. The non-rigid shape matching based on sparse spectral correspondence is presented in section 4. Experimental results are analyzed and discussed in Section 5. We conclude our work in Section 6.

2 Related work

2.1 Shape matching

An important work about shape matching is multidimensional scaling (MDS) proposed by Zigelman et al. [50] and Elad and Kimmel [16], they matched isometric shapes by embedding them into a Euclidian space, and implement a rigid shape matching in that space. Since it is generally impossible to embed a non-flat 2D manifold into a flat Euclidean domain without introducing some errors, Jain et al. [20], Mateus et al. [26] and Sharma and Horaud [37] suggested alternative isometry-invariant shape representations using eigendecomposition of discrete Laplace operators.

The spectrum of the Laplace operator provides large descriptive feature vectors, that is isometric-invariance, robust to local noise and sampling, shape-intrinsic, and multi-scale. Rustamov [33] proposed a Global Point Signature (GPS) for shape comparison by employing the discrete Laplace-Beltrami operator, which captures the shape's geometry faithfully. Ovsjanikov et al. [29] construct their Heat Kernel Signature (HKS) and Heat Kernel Maps, respectively. Zaharescu et al. [48] suggested an extension of 2D descriptors for surfaces, and used them to for shape matching. Hu and Hua [19] used the Laplace-Beltrami operator for matching using prominent features, and Dubrovina and Kimmel [14] suggested employing surface descriptors based on its eigendecomposition, combined with geodesic distances, in a quadratic optimization formulation of the matching problem. The above methods, incorporating pair wise constraints, tend to be slow due to high computational complexity.

Memoli and Sapiro, Bronstein et al., [5, 27, 28] compared shapes using different approximations of the Gromov-Hausdorff distance. Bronstein et al. [6] used diffusion geometry in order to match shapes with topological noise, and Thorstensen and Keriven [40] extended it to handle surfaces with textures. The GMDS algorithm [5] results in a non-convex optimization problem, therefore it requires good initializations in order to obtain meaningful solutions, and can be used as a refinement step for other shape matching algorithms. Anguelov et al. [1] optimized a joint probabilistic model over the set of all possible correspondences to obtain a

sparse set of corresponding points, and Tevs et al. [39] proposed a randomized algorithm for matching feature points based on geodesic distances between them. Zhang et al. [49] performed the matching using extrema curvature feature points and a combinatorial tree traversal algorithm, but its high complexity only allowed them to match only a small number of points. Moreover, there is no guarantee that this result minimizes the difference between pairwise geodesic distances of matched points. Instead of detecting the non-rigid mapping between two shapes, [21, 24, 30] search for a mapping from the shape to itself, and thus are able to detect intrinsic symmetries.

2.2 Shape correspondence

A recent survey of shape correspondence methods can be found in [41]. The most well-known approach is Iterative Closest Point (ICP) algorithm [2], which is used in [18] to align 3D shapes. However, this approach only computes rigid transformation for shape correspondence.

Recent works, most notably the TPS-RPM method of Chui and Rangarajan [7], attempt to incorporate non-rigid deformations into the ICP framework, using thin-plate splines (TPS) to model the deformation. To perform non-rigid alignment of shapes, some approaches embed the shapes in a common space to represent them. The most popular methods are Multi-Dimensional Scaling [50] and the spectral transform [16, 20, 26, 31, 32, 42, 44, 45]. Transforming a shape into the spectral domain can obtain a more intrinsic representation of the shape.

Computing a correspondence between shapes is one of the key problems that can benefit from semantically-driven techniques, some works segment a mesh into parts, finding analogies between these parts, transferring information or part styles [35, 36, 38], and using prior knowledge to learn how to label a shape or establish a correspondence [11, 22, 43]. Recently, some symmetry-aware algorithms have been proposed to improve the accuracy of intrinsic correspondence [34, 46, 47].

Our work is inspired by the spectral matching method [7, 42]. However, we find these methods are computationally costly because of the large number of dense points in each shape. So we propose a sparse graph representation method based on “Lewis weight” theory and MST; By using the multi-scale eigenfunctions it efficiently indicates the intrinsic structure among the deformable shapes. And eventually we apply TPS to implement shape similarity estimation and shape matching.

As it is shown in Fig. 1, our method takes a 3D mesh model as input. First, we combine the row sampling theory by Lewis Weights and polynomial approximation method to obtain a set of sparse and stable key points that are robust to noise and pose variance. Second, a sparse graph is constructed with the sampling points based on MST that compute the intrinsic affinity matrix efficiently. And then the 3D mesh is embedded in a sparse spectral space. Finally, the similarity between each two shapes is evaluated with the help of TPS method. A series of experimental results have shown the efficiency and accuracy of our method in similarity measurement and shape classification.

3 Sparse graph representation

3.1 Sparse sampling

Randomized sampling is an important tool in the design of efficient algorithms. A random subset often preserves key properties of the entire data set while allowing one to run algorithms

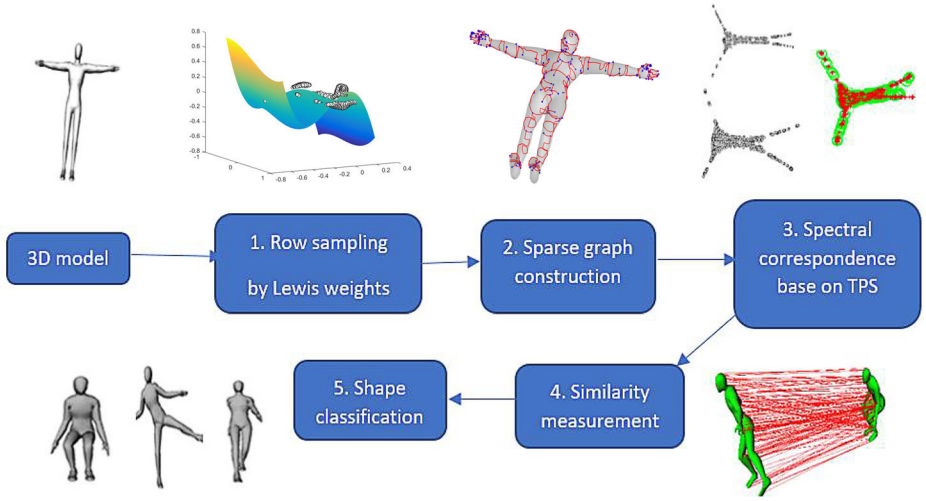

Fig. 1 Our method applies a two-stage sample-based approximation method to obtain stable key points and constructs a sparse graph; the efficient similarity is evaluated by a sparse spectral correspondence with the help of TPS

on a much smaller sample. Recently, row sampling of matrices has received much attention in numerical linear algebra [8, 10, 12, 13, 23].

Theorem 1. (Row sampling) *For a* $n \times d$ *matrix* $\boldsymbol{A}$ *where* $n > > d$ *and any error parameter* $\varepsilon > 0$, *we can find* A' *with a few (rescaled) rows of* $\boldsymbol{A}$.

$$\|Ax\|_p \approx_{1+\varepsilon} \|A'x\|_p \tag{1}$$

for all vectors $x \in R^d$. Here $\approx_{1+\varepsilon}$ denotes a multiplicative error between $(1+\varepsilon)^{-1}$and$(1+\varepsilon)$. Let n and d to denote number of rows and columns respectively, and $a_i$to denote the vector corresponding to the i^{th}row of $\mathbf{A}$. A crucial definition in ℓ_2 row sampling and matrix concentration bounds is statistical leverage scores τ_i:

$$\tau_i(A) \overset{def}{=} a_i^T \left(A^T A\right)^{-1} a_i = \left\| \left(A^T A\right)^{-1/2} a_i \right\|_2^2 \tag{2}$$

The well-known sampling results for general ℓ_p norms [8–10, 13], are based on a "change of density" construction originally due to Lewis [23]. This construction assigns weights w_i, analogous to a leverage score, to each row a_i; these weights can be used directly as the sampling probability.

Theorem 2. (Lewis Weight) *For a matrix* $\boldsymbol{A}$ *and norm p, the* ℓ_p*Lewis weights* $\overline{w}$ *are the unique weights such that for each row i we have* $\overline{w} = \tau_i\left(\overline{W}^{1/2-1/p} A\right)$ *or* $a_i^T \left(A^T \overline{W}^{1/2-1/p} A\right)^{-1} a_i = \overline{w}_i^{2/p}$ [9].

Note that for the case where $p = 2$, that is ℓ_2, $W^{1/2-1/p}$ is the identity matrix, so the Lewis weights are just the leverage scores.

Drineas etc. [12] solve a sampling algorithm and corsets for ℓ_p regression based on "Lewis Weight" theory, and provide a well-conditioned basis to obtain an exponentially better "condition number".

Theorem 3. (ℓ_p regression problem) *Let* $\|\cdot\|$ *denote the p-norm of a vector. Given as input a matrix* $A \in R^{n \times m}$, *a target vector* $b \in R^n$, *and real number* $p \in [1, \infty)$, *find a vector* x_{OPT} *and a number Z such that*

$$Z = \min_{x \in R^m} \|Ax - b\|_p = \|Ax_{OPT} - b\|_p \tag{3}$$

Theorem 4. (well-conditioned basis) *Let* $\boldsymbol{A}$ *be an* n × d *matrix of rank d, let* $p \in [1, \infty)$, *let q be its dual norm, where* $1/p + 1/q = 1$, *then an* n × d *matrix* $\boldsymbol{U}$ *is an* (α, β, p)*-well-conditioned basis for the column space of A if the columns of* $\boldsymbol{U}$ *span the column space of* $\boldsymbol{A}$ *and (1)* $\|\|U\|\|_p \le \alpha$, *and (2) for all* $z \in R^d$, $\|z\|_q \le \beta \|Uz\|_p$. *We will say that* $\boldsymbol{U}$ *is a p-well-conditioned basis for the column space* $\boldsymbol{A}$ *if* α *and* β *are* $d^{O(1)}$, *independent of m and n. If* $p < 2$, *then* $\alpha = d^{\frac{1}{p}+\frac{1}{2}}$ *and* $\beta = 1$; *if* $p = 2$, *then* $\alpha = d^{\frac{1}{2}}$ *and* $\beta = 1$; *and if* $p > 2$, *then* $\alpha = d^{\frac{1}{p}+\frac{1}{2}}$ *and* $\beta = d^{\frac{1}{q}-\frac{1}{2}}$ [12].

The significance of a *p*–well-conditioned basis is that it is able to minimize the variance in sampling process by randomly sampling rows of the matrix **A** and elements of the vector *b* according to a probability distribution that depends on norms of the rows of the matrix **U**. This will allow us to preserve the subspace structure of span (**A**) and thus to achieve an$(1 + \varepsilon)^{-1}$-approximation to the ℓ_p regression problem more efficiently.

In this paper we adopt the ℓ_p regression algorithm [12] and "Lewis weights" theory [9] to efficiently extract the key sample points over 3D mesh model.

We define a polynomial surface and compute the importance of each point in a mesh model for surface approximation by solving a ℓ_2 regression problem. The importance of each point is used as sampling probability to extract key sample points. We demonstrate the two-stage approximation algorithm and the sampling results to prove the efficiency and robustness of our sampling method.

3.2 Sparse sampling by Lewis weights

An important question in algorithmic theory is whether there exists a *small* subset of the input such that if computations are performed only on this subset, the solution to the given problem can be *approximated* well.

In this paper, we adopt a two-stage sampling-based approximation algorithm to obtain the key sample points from a mesh model [12]. The first stage of the algorithm is sufficient to obtain a constant factor approximation to a polynomial surface. The second stage of the algorithm carefully uses the output of the first stage to construct a coreset and achieve arbitrary constant factor approximation, which can be considered as sampling probability.

Assume that we have a series of points $A = \{(x_1, y_1, z_1), \ldots (x_n, y_n, z_n)\}$, and an approximat polynomial surface $f(x, y)$ of degree d:

$$z = f(x,y) = \sum_{i+j\le d} c_{i,j} x^i y^j \tag{4}$$

And all these polynomials constitute a linear space S_d:

$$S_d := \{f(x,y) | \deg f(x,y) \le d\} \tag{5}$$

The distance between point and surface f is defined as:

$$distance(A, f) := \sqrt{\sum_{i=1}^{n} (z_i - f(x_i, y_i))^2} \tag{6}$$

Then there exists a unique $f_0(x, y)$ that satisfies:

$$distance(A, f_0) := \min_{f \in S_d} distance(A, f) \tag{7}$$

So the greater the value of d is, the better the surface $f_0(x, y)$ approximates the set **A**. We now can rewrite *distance*(A, *f*) as matrix format:

$$distance(A, f) = \sqrt{\sum_{i=1}^{n} (z_i - f(x_i, y_i))^2} = \sqrt{\sum_{i=1}^{n} \left(z_i - \sum_{i+j\le d} c_{i,j} x_i y^j\right)^2} \text{ Define}$$

$$B = \begin{pmatrix} 1 & x_1 & y_1 & x_1^2 & x_1 y_1 & y_1^2 & \cdots & x_1^d & x_1^{d-1} y_1 & \cdots & y_1^d \\ 1 & x_2 & y_2 & x_2^2 & x_2 y_2 & y_2^2 & \cdots & x_2^d & x_2^{d-1} y_2 & \cdots & y_2^d \\ \vdots & \vdots & \vdots & \vdots & \vdots & \vdots & \ddots & \vdots & \vdots & \vdots & \vdots \\ 1 & x_n & y_n & x_n^2 & x_n y_n & y_n^2 & \cdots & x_n^d & x_n^{d-1} y_n & \cdots & y_n^d \end{pmatrix} \quad C = \begin{pmatrix} c_{0,0} \\ c_{1,0} \\ \vdots \\ c_{0,d} \end{pmatrix} \quad Z = \begin{pmatrix} z_1 \\ z_2 \\ \vdots \\ z_n \end{pmatrix} \tag{8}$$

Now the *distance*(A, *f*) can be written as:

$$distance(A, f_0) = \|BC - Z\|_2 \tag{9}$$

Matrix C is the coefficients of polynomial surface f and ordered in sequence, and we have:

$$\min_{f \in S_d} distance(A, f) = \min_{C \in R_{\frac{(d+1)(d+2)}{2}}} \|BC - Z\|_2 \tag{10}$$

Here $R_{\frac{(d+1)(d+2)}{2}}$ is the $\frac{(d+1)(d+2)}{2}$ Euclidean space.

Ideally, there exists a C_0 to satisfies $BC_0 = Z$ which makes all points of A fitting the polynomial surface $f_0(x, y)$, but for a fixed d, it becomes an over-determined problem since the number of rows of matrix B is often far bigger than the number of columns, that is $n >> d$. It means that a few rows of the matrix B play an important role for the **$\ell_p$regression problem** as described in the Theorem1.3. Hecne we can use row sampling to solve this approximation problem.

In this paper we use a two-stage row sampling algorithm to sample the matrix and the corresponding optimal solution is between $(1+\varepsilon)^{-1}$ and $(1+\varepsilon)$ [9, 12].

Given a mesh M with n points, and an approximated polynomial surface f, we build the matrix **B** (Eq. 8). The row sampling algorithm takes as input an $n \times m$ matrix **B** of rank d, a target vector $z \in R^n$. And a number $p = 2$ means ℓ_2 regression problem. It returns vector $q_i \in R^m$ as Lewis weight to each row, which is used as the sampling probability.

Algorithm 1: Row sampling by Lewis Weights

Input: A matrix $B \in R^{n\times m}$, a vector $z \in R^n$.

Let $0 < \varepsilon < 1/7$ and k=2;

Output: Lewis weight to each row q_i

Find a p-well-conditioned base $U \in R^{n\times d}$ for span B (p=2).

Step1:

(1) Define $p_i = \min\left\{1, \frac{\|U_{i*}\|}{\|U\|_p^p} r_1\right\}$, where $r_1 = 16(2^p+2)d^k(d\ln(8\cdot 12)+\ln(200))$.

(2) Generate (implicitly) S where $S_{ii} = 1/p_i^{1/p}$ with probability p_i and 0 otherwise.

Let $\hat{x}_c$ be the solution to $\min_{x\in R^m} \|S(Bx-z)\|_p$

Step2:

Let $\hat{\rho}_c = B\hat{x}_c - z$ and unless $\hat{\rho}_c = 0$, define $q_i = \max\left\{p_i, \frac{|\hat{\rho}_i|^p}{\|\hat{\rho}\|_p^p} r_2\right\}$ with $r_2 = \frac{150\cdot 24^p d^k}{\varepsilon^2}(d\ln(\frac{280}{\varepsilon})+\ln(200))$.

Output q_i

The algorithm first computes a p–well-conditioned basis $\boldsymbol{U}$ for span ($\boldsymbol{B}$), as described in the Theorem1.4. Then, it uses information from the norms of the rows of $\boldsymbol{U}$ to sample constraints from the input ℓ_p regression problem. In particular, roughly $O(dp+1)$ rows of **B**, and the corresponding elements of z, are randomly sampled according to the probability distribution given by

$$p_i = \min\left\{1, \frac{\|U_{i*}\|}{\|U\|\|_p^p} r_1\right\}, \text{where } r_1 = 16(2^p+2)d^k(d\ln(8\cdot 12)+\ln(200)). \quad (11)$$

In our method, we choose $p = 2$ and solve a ℓ_2 regression problem. We use S to denote the sampling matrix for the first-stage sampling probability.

In the second stage, we use the output from the first stage to refine the sampling probability.

$$q_i = \max\left\{p_i, \frac{|\hat{\rho}_i|^p}{\|\hat{\rho}\|_p^p} r_2\right\}, \text{where } r_2 = \frac{150\cdot 24^p d^k}{\varepsilon^2}\left(d\ln\left(\frac{280}{\varepsilon}\right)+\ln(200)\right). \quad (12)$$

And the constant factor q_i as Lewis eight of each row is finally obtained which represents the importance for the approximation.

The ultimate goal of row sampling is to evaluate the importance of each point to the approximated surface. And it is obvious that the points approximate well when the degree d is larger (see Fig. 2). We choose $d = 6$ as a trade off in our experiments.

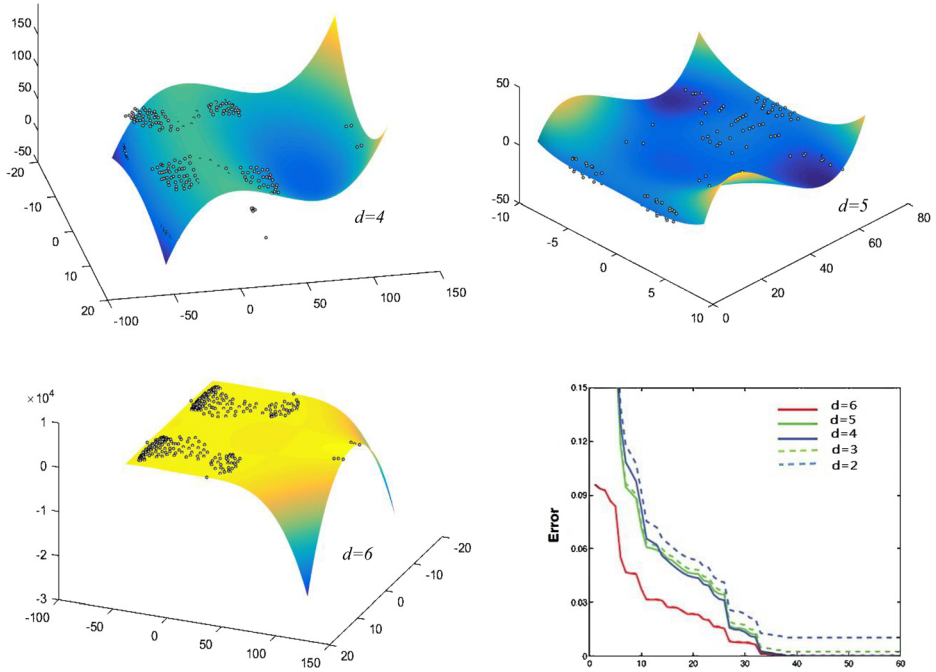

Fig. 2 The polynomial surface of degree d ($d = 4, 5, 6$) and the approximation errors

All the points in the matrix are reordered with Lewis weight q_i in descending order, and then the key sample points can be selected according to user's choice. In our experiments we set $\varepsilon = 0.01$, and as we can see in Fig. 3a key sample points (black balls) are extracted with different sparse ratio $\tau = 0.1$, $\tau = 0.2$, $\tau = 0.5$.

To evaluate the sampling results it usually needs two kinds of metrics: the control metric r and the distance metric d_m. The control metric r reflects the user preferences of the sampling pattern, such as density, adaptivity. The distance metric d_m reflects properties of the underlying sample space Ω, essentially defining the distance between any pairs of samples within Ω [15]. It is usually used to evaluate the stability of sampling method.

Here we define the distance between the pair of sample points $d(s_1, s_2)$ via the surface geodesic and let r be the distribution of the histogram of geodesic distance which indicates the sampling density.

We normalize the geodesic distance between all pairs of sample points and divide the normalized geodesic distance into five ranges; the distribution of sample points in each range is calculated as shown in histogram in Fig. 3a, we can see that our method obtain the similar density distribution r of geodesic distance even with different sparse ratio τ. It effectively reveals the stability of the sample space.

Figure 3b shows the comparison of sampling results, our sample points indicate better structural distribution than those based on salient geometric sampling (SGS) method [17] and MLS method [3], and it achieves similar simplified results with fewer sample points comparing with Poisson disk (PD) method [4, 15]. In Fig. 3c we can see our sampling method is robust to the Gaussian noise ($\delta = 0.0015$) and the distribution density of sample points in human model with sparse ratio $\tau = 0.3$ is very stable.

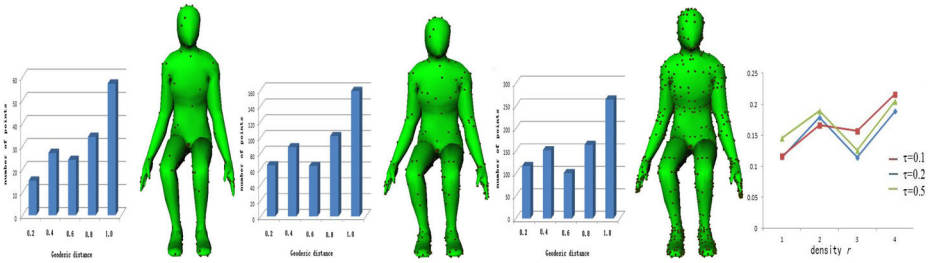

(a) The key points extraction with sample rates τ=0.1, τ=0.2, τ=0.5 by our method

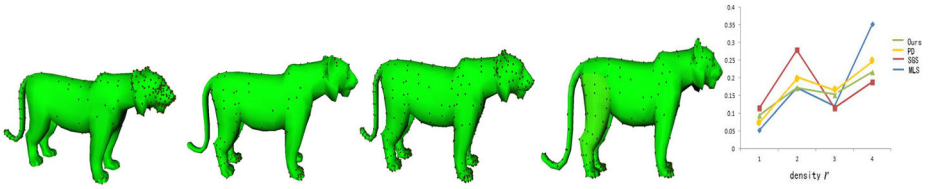

(b) sampling results based on SGS[39] , MLS[40] , PD [41] and ours.

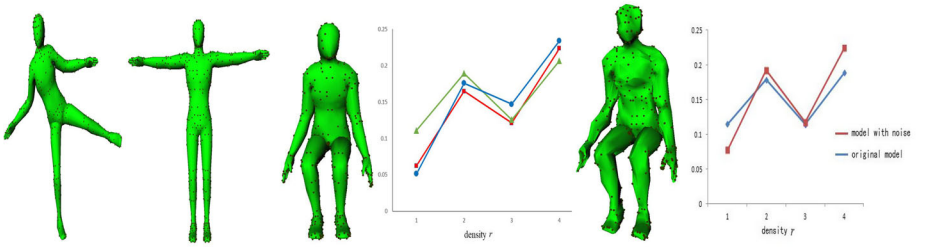

(c) sampling results on different poses of human models and with Gaussian noise (δ=0.0015)

Fig. 3 The comparison of sampling results. (**a**) The key points extraction with sample rates $\tau = 0.1$, $\tau = 0.2$, $\tau = 0.5$ by our method. (**b**) sampling results based on SGS [17], MLS [3], PD [4] and ours. (**c**) sampling results on different poses of human models and with Gaussian noise ($\delta = 0.0015$)

3.3 Sparse graph construction with MST

We build a sparse weighted graph representation for each mesh model with key sample points by using minimum spanning tree (MST) algorithm.

Given a mesh model $G = \langle V, E \rangle$, we construct the shortest path $P_{ij}^{(k)} | \underbrace{v, \ldots v_j}_{k} \in V$ for each pair of key sample points (v_i, v_j) (see Fig. 4), k is the number of the points on this shortest path, and then the weight for this path can be evaluated as $w_{ij}^{(k)}$:

$$w_{ij}^{(k)} = \begin{cases} 1 & i = j \\ dt_{ij} & k = 0; i \neq j \\ \min\left(dt_{ij}^{(k-1)}, dt_{ik}^{(k-1)} + dt_{kj}^{(k-1)}\right) & k \geq 1; i \neq j \end{cases} \tag{13}$$

Here dt_{ij} is the Euclidean distance between adjacent points (v_i, v_j), $\min\left(dt_{ij}^{(k-1)}, dt_{ik}^{(k-1)} + dt_{kj}^{(k-1)}\right)$ means iteratively computing the distance of each pair of adjacent

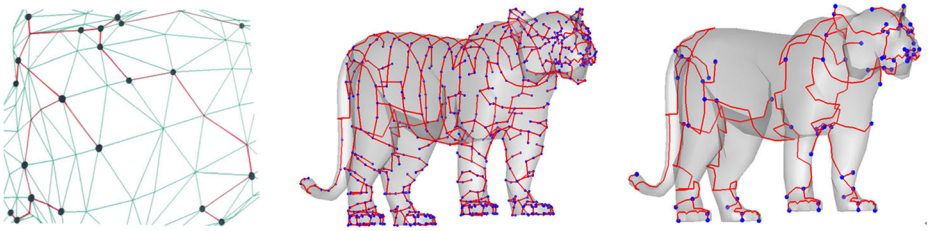

Fig. 4 The Sample points and the sparse graphs with MST ($n = 800$; $n = 200$)based on different sparse ratios: $\tau = 0.7$; $\tau = 0.3$

points on the shortest path between two sample points (v_i, v_j). Based on MST a sparse weighted graph G′=⟨V′, E′, W⟩ and its affinity matrix $\boldsymbol{W}$ are finally constructed.

Algorithm 2: Sparse graph construction with MST.

Input: Mesh model $G=\langle V \in R^n,\ E\rangle$ and sample points $V' \in V$

Output: **MST** $G'=\langle V_{new}, E_{new}\rangle$ and affinity matrix W

Initialize: $V_{new}=v_1, v_1 \in V'$, $E_{new} \leftarrow null$, m is the number of sample points $m < n$.

For i=1 , … m do

$V_i \in V$; $V_i \notin V_{new}$

For j=1 , … n do

$if(i = j)$ $w_{ij}^{(k)}=1$;

$if((i \neq j)\&\&\ (k=0))$ $w_{ij}^{(k)}=dt_{ij}$; // (v_i, v_j) is a pair of adjacent points.

$if((i \neq j)\&\&\ (k \geq 1)\&\&(V_k \notin V'))$

$w_{ij}^{(k)}=\min(dt_{ij}^{(k-1)}, dt_{ik}^{(k-1)}+dt_{kj}^{(k-1)})$; $V_{new} \xleftarrow{add} V_k$ $E_{new} \xleftarrow{add} E_{ij}$;

Endfor

Endfor

Output $G'=\langle V_{new}, E_{new}, W\rangle$

Fig. 4 has shown the key sample points by Lewis Weights and a constructed sparse graph by using MST.

Since Laplace-Beltrami spectrum reveals intrinsic structure and morphology of the deformable shape, It provides a robust tool for shape analysis [19, 29, 33, 48].

Therefore, we embed our MST into spectral space to build sparse spectral representation in order to find intrinsic similarities among shapes.

The affinity matrix W of MST is eigendecomposed as $W = Q\Lambda Q^T$, Λ is a diagonal matrix where the diagonal elements ($\lambda_1 \geq \ldots \lambda_n$) are the eigenvalues and sorted in descending order. $Q = [v_1 \cdots v_l]$ is a $l \times l$ matrix and $v_1, \cdots v_l$ are eigenvectors corresponding to the eigenvalues.

We choose the first k largest dimension eigenvector Q_k for the corresponding ordered eigenvalues. The row vectors of Q_k can be regarded as the embedding coordinates of the corresponding points in the k-dimensional spectral domain.

Figure 5 shows *2*-dimensional eigenmaps of human model (with the 2nd, 3rd largest eigenvalues) with 100 and 30% sample points. We can see that our sparse spectrum keeps well structural description.

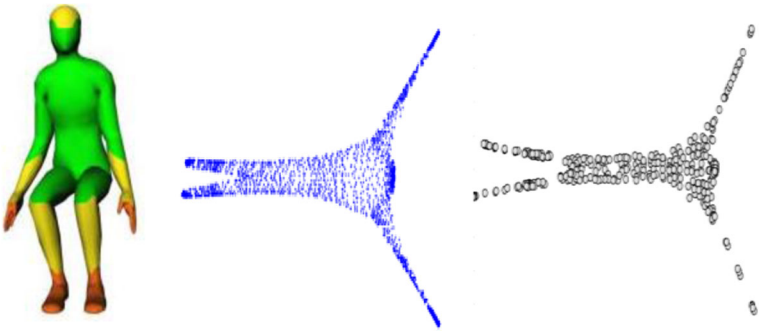

Fig. 5 Human model and its 2-D spectral eigenmap with different sample points ($\tau = 1.0$, $\tau = 0.3$)

4 Shape correspondence based on sparse spectral embedding

The purpose of transforming the 3D mesh from the spatial domain to the *k-D* spectral domain is to attain invariance to isometric transformation, and uniform scaling, as well as robustness to difference in mesh sizes.

In this work, we match each pair of sparse graphs that we constructed with spectrum by TPS transformation [7].

Given two sparse spectral embeddings $\hat{A}$ and $\hat{B}$, the transformation function $g : \hat{A}_i \in R^k \rightarrow \hat{B}_j \in R^k$ maps a point set in *2* dimensional space to another point set by minimizing the following energy function:

$$E(g) = \sum_{j=1}^{n} \|\hat{A}_i - g(\hat{B}_j)\| + \beta \iint \left[\left(\frac{\partial^2 g}{\partial x^2} \right)^2 + 2 \left(\frac{\partial^2 g}{\partial x \partial y} \right)^2 + \left(\frac{\partial^2 g}{\partial y^2} \right)^2 \right] dxdy \tag{14}$$

where β is the regularization (smoothing) parameter. Assume that the correspondence between $\hat{A}$ and $\hat{B}_j$, the point $\hat{B}_j$ is the matching point for $\hat{A}_i$. The unique g that minimizes the above energy function has the form:

$$g(\hat{B}_j, t, w) = \hat{B}_j \cdot t + \sum_{i=1}^{m} w_i \cdot \varphi\left(\|(x_i, y_i) - \left(x_j, y_j\right)\| \right) \tag{15}$$

Where $\boldsymbol{t}$ is an $(k+1) \times (k+1)$ affine coefficient matrix and $\boldsymbol{w}$ is a $n \times (k+1)$ non-rigid warping coefficient matrix. φ is the TPS kernel, $\varphi(r) = r^2 \log r^2$, $r = \|(x_i, y_i) - (x_j, y_j)\|$. The coefficients of $\boldsymbol{t}$ and $\boldsymbol{w}$ can be calculated with

$$\begin{bmatrix} K & \hat{B}^T \\ \hat{B} & 0 \end{bmatrix} \begin{bmatrix} w \\ t \end{bmatrix} = \begin{bmatrix} \hat{A} \\ 0 \end{bmatrix} \tag{16}$$

where $K_{ij} = \varphi(\|(x_i, y_i) - (x_j, y_j)\|)$.

Using this transformation form, we transform the point set $\hat{A}$ to point set $\hat{B}$. This process is iterated until convergence. We have found experimentally that 5 to 10 iterations of the iterative alignment are sufficient to align the embeddings. The value of the regularization parameter β is set to be the mean distance between all embedded point pairs. Finally, we can obtain the distance of each matching point pairs $\left(a_i{}^{(M_1)}, b_i{}^{(M_2)}{}_{C(i)} \right)$, $a_i{}^{(M_1)}$ is the i^{th} vertex of spectral embedding $\hat{A}$ and $b_i{}^{(M_2)}{}_{C(i)}$ is the $C(i)^{th}$ vertex of spectral embedding $\hat{B}$, where C is the correspondence found by our algorithm.

This way, we use the sum of squared difference (SSD) and the correlation coefficient (CC) as evaluation parameters of shape matching (Eqs. 18, 19). The larger value of SSD represents the worse correspondence, but the larger CC will show the better shape similarity. Consequently, the matching accuracy $sim(M_i, M_j)$ between each two mesh models can be computed (Eq. 20).

$$C_i = \mathrm{argmin}_j \|\hat{A}_i - \hat{B}_j\|; \tag{17}$$

$$SSD = \left(\sum_{i=1}^{N} \left({a_i}^{(M_1)} - {b_i}^{(M_2)}{}_{C(i)} \right)^2 \right)^{1/2} / N; \tag{18}$$

$$CC = \frac{\sum_{i=1}^{N} \left(a_i^{(M_1)} - \overline{\alpha}^{(M_1)} \right) \left(b_i^{(M_2)}{}_{C(i)} - \overline{\beta}^{(M_2)}{}_{C(i)} \right)}{\left(\sum_{i=1}^{N} \left(a_i^{(M_1)} - b_i^{(M_2)}{}_{C(i)} \right)^2 \right)^{1/2}} \tag{19}$$

Where $\overline{\alpha}$ and $\overline{\beta}$ are the mean distances of $\hat{A}$ and converted $\hat{B}$ respectively. We set a threshold parameter $\gamma = 0.05 \cdot \left(\overline{\alpha} + \overline{\beta}\right) / 2$, for each matching point pair $\left({a_i}^{(M_1)}, {b_i}^{(M_2)}{}_{C(i)} \right)$, if $\|a_i^{(M_1)} - b_i^{(M_2)}{}_{C(i)}\| \le \gamma$, it is an effective matching pair, if $\|a_i^{(M_1)} - b_i^{(M_2)}{}_{C(i)}\| > \gamma$, then it is not effective matching pair. We can then obtain the matching accuracy $sim(M_i, M_j)$ of each two 3D models M_i and M_j, N_{eff} is the number of the effective matching pairs, m, n is the number of points in M_i and M_j respectively.

$$sim\left(M_i, M_j\right) = \frac{N_{eff}}{\min(m, n)} \tag{20}$$

Figure 6 has shown the results of sparse spectral correspondence, we first create affinity matrix for each sparse graph, and then build a sparse spectral eigenmap (see Fig. 6b). The shape correspondences are finally obtained in a spectral domain (see Fig. 6c). Figure 6d shows the shape alignment in spatial domain which is difficult to reveal the consistency of non-rigid shapes.

Clearly, our algorithm can effectively recognize the same category meshes. And it behaves robustly against moderate stretching and pose-variance in shapes.

To summarize, the procedure of our spectral correspondence is described in Algorithm 3.

Algorithm 3: Procedure of spectral correspondence.

Input: a set of 3D weighted graph from different classes: $\boldsymbol{S}$

Output: optimal shape classification: $s_k \in S$

1. Construct sparse graph representation for each shape $\boldsymbol{S_i}$ by extracting key sample points.

2. Construct an affinity matrix and compute W_i for each shape $\boldsymbol{S_i}$ with MST.

3. Embed each matrix W_i in the spectral domain, initialize the affine transformation matrix $\boldsymbol{t_i}$, warping coefficients matrix $\boldsymbol{w_i}$ and the smoothing parameter β_i. Perform TPS method to align and match the spectral embedding.

4. Compute the squared distance (*SSD*), the correlation coefficient (CC) and the matching accuracy $sim(S_i, S_j)$ between each two input shapes.

6. Sorting all the input shapes from high to low based on *CC*, and output top ranking of input shapes as the same category $s_k \in S$.

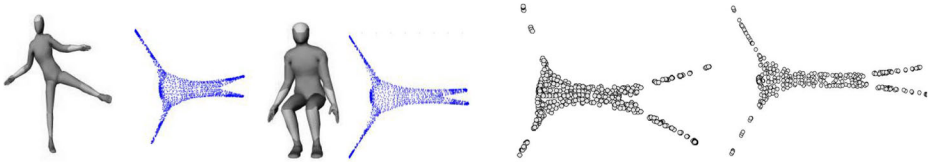

(a) The spectral eigenmap of two human models (b) Sparse spectral eigenmap with sparse ratio $\tau = 0.3$

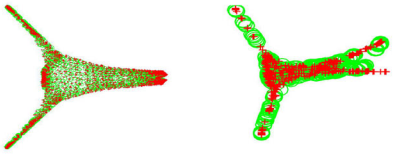

(c) Sparse spectral correspondence based on TPS

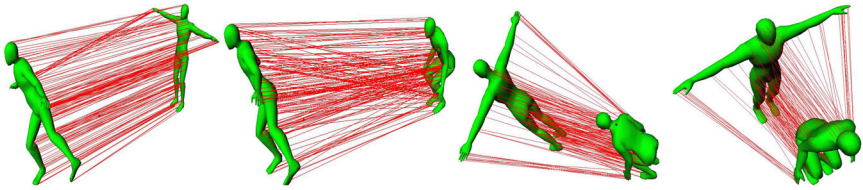

(d) Non-rigid shape matching based on sparse spectral correspondence

(e) shape alignment in spatial domain

Fig. 6 The shape matching results based on sparse spectral correspondence. (**a**) The spectral eigenmap of two human models (**b**) Sparse spectral eigenmap with sparse ratio $\tau = 0.3$. (**c**) Sparse spectral correspondence based on TPS. (**d**) Non-rigid shape matching based on sparse spectral correspondence. (**e**) shape alignment in spatial domain

5 Experimental results

In this work, we develop a row sampling and sparse graph construction method to generate a sparse descriptor for most of shapes which is useful for shape matching and analysis.

In this section, we demonstrate experimental results and analyze the performance of our algorithm. We choose Princeton Segmentation Benchmark as our test set. All experiments are performed on Intel Core™ CPU 3.5 GHz, 8GB memory.

The time complexity of our algorithm is mostly dependent on the shape resolution. In our method we firstly implement a row sampling to reduce resolution of complex shapes to less than 2 K points. At the same time, the subsampled points can maintain well the geometrical and topological properties for most of shapes.

We assume that the input shape with n points. In the sampling stage, suppose that the average number of sample points is N_k ($N_k < n$), then the sampling procedure is $O(nd^2 \log(n))$, where $d = \text{rank}(B)$, and the computing of sparse graph and spectral embedding takes $O(N_k \log(N_k))$.

Table 1 The performance of our method (s: seconds)

Models (points)	Sample points (s)	MST + spectral embedding (s)	Sparse spectral matching (s)
Humans (3206)	17.25	6.63	12.6
Cat (1730)	10.21	3.08	6.4
Planes (1038)	5.74	2.01	5.02
Fishes (563)	1.98	1.22	2.26
Horses (69451)	25.24	17.94	68. 47
Tiger (2834)	15.31	12.64	20.05
Camel (2830)	14.46	12.45	19.39
Wolf (1243)	12.58	4.37	8.46
Cow (2903)	16.31	12.96	20.21

The spectral correspondence algorithm is dependent on initializing the affinity matrix. For a pair of shapes, the computation complexity of shape matching is $O\left(N_k^2 \log(N_k)\right)$.

Table 1 has shown the efficiency of our method. The longest processing time is almost 2 min for the horse's category since it has the greatest number of points in the model and the shortest processing time is 5 s for the fish category. Figure 7 demonstrates the sparse spectral correspondence results with different sparse ratio (the third column: $\tau = 0.2$, the forth column: $\tau = 0.5$) for deformable shapes.

Table 2 provides a general comparison of the average accuracy of classification with other methods. Although spectral embedding takes large computational time because of the eigen-decomposition of large dense matrices, our method effectively reduces the size of input shapes by extracting the key sample points and the sparse spectral embedding generates a better shape descriptor. Experimental results have proved that our method achieves better accuracy rates of classification than the others (see Fig. 8).

Because this algorithm defines a sparse ratio τ to build sparse representation of the model, the choice of parametersτ may affect the classification accuracy; therefore the influence of the parameter values τ was tested in our experiments. We chose eight equidistant distributions

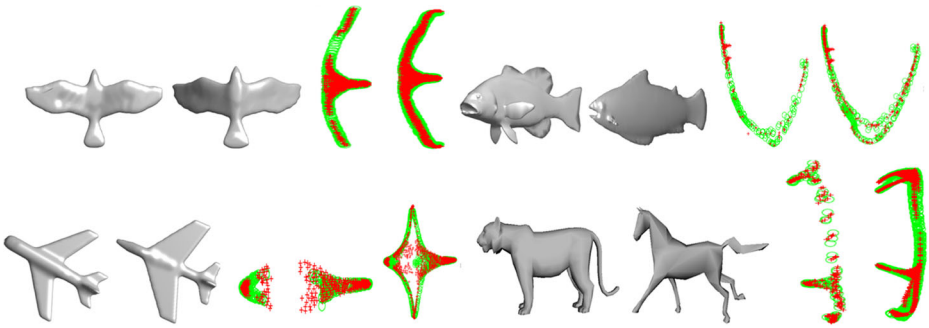

Fig. 7 Sparse spectral correspondence for mesh models

Table 2 The average classification accuracy of our method on different shape categories (%)

Category	Ours	MDS [50]	ICP [2]	Parts [25]	TP S - RPM [7]
Humans	86.75	83.69	84.69	86.45	86.51
Four-legged animals	89.94	83.75	89.74	84.32	89.86
Airplanes	88.67	83.27	86.52	88.41	88.36
Birds	81.58	80.28	81.69	82.63	80.92
Fishes	72.32	71.57	70.86	70.96	72.24
Cups	66.87	67.38	65.41	60.24	66.97

between$\tau = 0.1$~0.8, the average recognition accuracy on all models are calculated respectively as shown in Fig. 9b.

In order to test the robustness of our algorithm, we use Gaussian noise on the 3D models (Fig. 9c). The shape matching result still keeps the roughly the same accuracy. The horizontal axis indicates the intensity of Gaussian noise added, increasing the noise intensity from 0.1 to 1%. Longitudinal axis is the average recognition rate of the model under different noise intensity in all tests. When the noise intensity is below 0.2%, the average recognition rate of the algorithm can keep the high accuracy even with different sampling rate; when the noise intensity is more than 0.2%, the recognition rate increases with the increase of τ. Overall, as the noise intensity increases, the average recognition rate of the model gradually declines.

Figure 9d demonstrates the stable shape matching results between 3D models with Gaussian noise added. We add $\delta = 0.0015$ Gaussian noise on these human models, and build the sparse representation by our row sampling ($\tau = 0.3$), the shape similarity is revealed through the sparse spectral correspondence as shown in the fourth and fifth columns in Fig. 9d, from which the similarity estimation is obtained. The matching rates between these 3D models are 96.75 and 94.13% respectively. It verifies that our method is effective and robust to the noise and deformation. We further tested our method for incomplete models, as shown in Fig. 9e. The similarity between two incomplete models is well recognized by using the sparse spectral correspondence.

Table 3 demonstrates the representative matching results produced by our approach on the 16 categories from the PSB. We take a mesh model as the query shape and apply our sparse

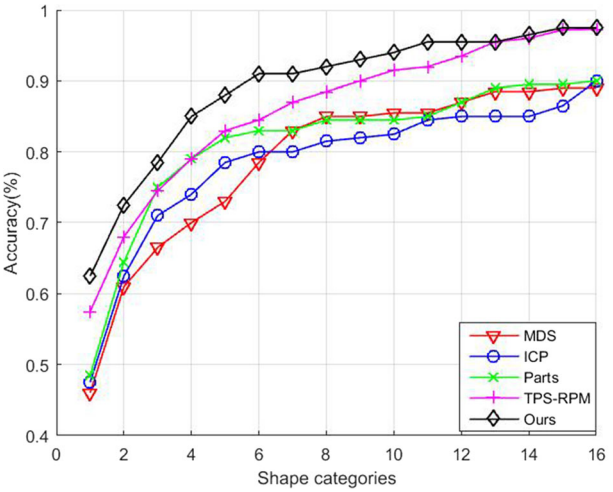

Fig. 8 The comparison of classification accuracy with other methods

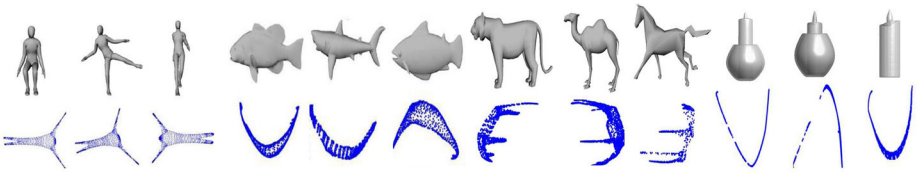

(a) The sparse spectrum of 3D models with τ=0.8

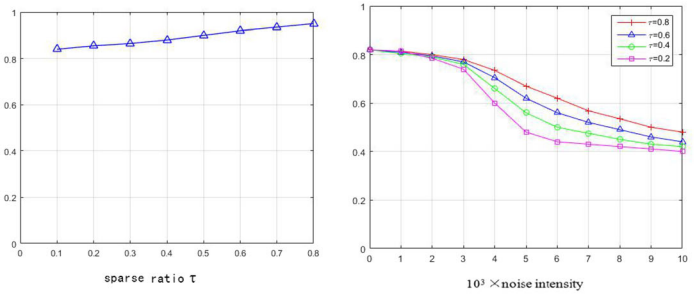

(b) The average recognition accuracy on all models with different sample rates (c) the effect of Gaussian noises

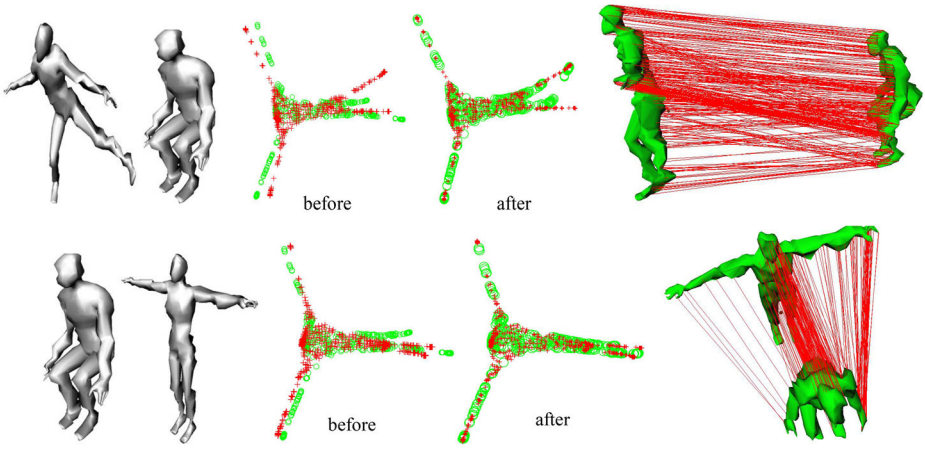

(d) The shape matching with Gaussian Noise (δ = 0.0015)

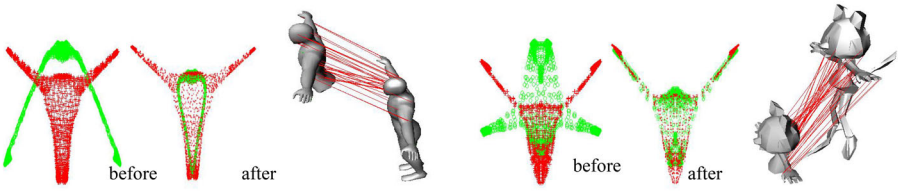

(e) The shape matching with incomplete models

Fig. 9 The experimental results of our method. (**a**) The sparse spectrum of 3D models with $\tau = 0.8$. (**b**) The average recognition accuracy on all models with different sample rates (c) the effect of Gaussian noises. (**d**) The shape matching with Gaussian Noise ($\delta = 0.0015$). (**e**) The shape matching with incomplete models

sampling and spectral matching method to evaluate the similarity in the database, and the most similar candidates (top 3 ranking models sorted by CC value) are obtained. From the

Table 3 Non-rigid Shapes Similarity Analysis

Name	Model	Name	Model
Human		Bird	
Ant		Hand	
Candle		Spider	
Fish		Glass	
Horse		gorilla	
Rabbit		triceratops	
plane		piles	
dog		cat	

experiment results we can find that our algorithm can accurately identify similar shapes on a large variety of categories of shapes, even though the input shapes undergo large deformation in geometric structure. The algorithm has good recognition accuracy. In the 16 categories of 3D models, the majority of the models have more than 95% accuracy, and the average recognition accuracy of all models is 88.5%.

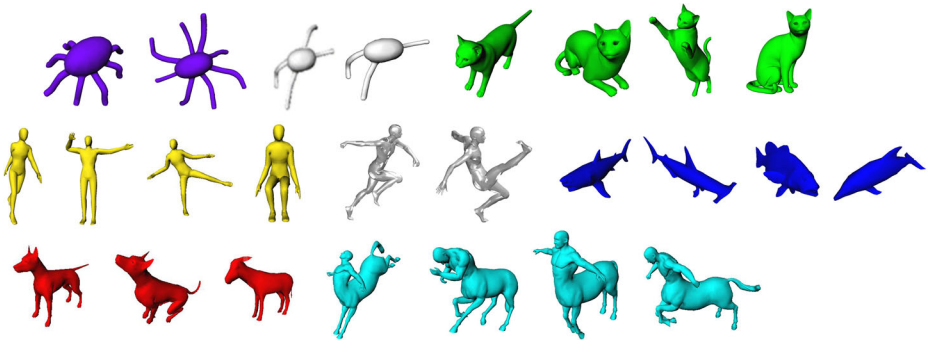

Fig. 10 An example of shape classification of the dataset, obtained by running our similarity measurement algorithm. Classes are encoded by color; note that two incomplete octopus and two human models with holes (in gray) have been left unmatched

6 Conclusions and future work

In this paper, we present an efficient approach to find the similarity between 3D shapes. We first build a sparse representation for each input shape by extracting a subset of key sample points under the "Lewis Weight" constraint. And then we generate a sparse graph with MST. After transformation from spatial domain to the spectral domain, match of the spectral embeddings are constructed to ensure a consistent ordering and sign assignment of the eigenvectors with TPS method. Our algorithm is robust against differences in mesh sizes and choice of the dimensionality of the embeddings. It is invariant under isometric transformation. Experimentally, we find it to be robust against moderate stretching in the shapes as well, and it outperforms well-known existing shape correspondence schemes. The complexity for computing the spectral embeddings and the correspondence is $O(N_k^2 \log N_k)$, where N_k is the average number of sample points in the larger mesh.

However, similar to the spectrum analysis methods, our method also relies on the computation of geodesics, we require the shape to have no significant missing parts, although our sparse model can successfully deal with partial similarity, this partiality is not easily controllable. An example is shown in Fig. 10, where two octopus are left unmatched by our method, and the human models with large holes are not matched either.

In the future we would like to extend the scope of the structure-based and semantic-based shape descriptors for more efficient shape matching instead of time consuming point matching. Furthermore, we will investigate shape co-segmentation for the application of shape retrieval.

Acknowledgements We would like to express our gratitude to the anonymous reviewers for their helpful comments. The research presented in this paper is supported by a grant from NSFC (61702246), fund of CSC (201608210289) and an Education. project of Liaoning Province (2018lsktyb-084). We are also highly thankful to Hong Kai Zhao, the Professor of department of Mathematics, University of California Irvine, for inspiring guidance of derivation of mathematic formulas. We sincerely appreciate Qiao Long Huang, the PhD student of IMSS, Chinese Academic of Sciences who helped us to verify the feasibility of our sampling algorithm, and Rui Xiang, the PhD student of department of Mathematics, University of California Irvine for his effort in analyzing the shape matching results.

References

1. Anguelov D, Srinivasan P, Pang H-C, Koller D, Thrun S (2004) The correlated correspondence algorithm for unsupervised registration of nonrigid surfaces. In: Proceedings of the neural information processing systems (NIPS) conference, vol 17. MIT Press, Cambridge, pp 33–40
2. Besl P, McKay N (1992) A method for registration of 3-D shapes. IEEE Trans Pattern Anal Mach Intell 14(2):239–256
3. Bremer PT, Hart JC (2005) A sampling Theorem for MLS surfaces. In Proceedings of Symposium on Point - Based Graphics 47–54
4. Bridson R (2007) Fast Poisson disk sampling in arbitrary dimensions. In Proc. ACM SIGGRAPH 2007 Sketches, Article No. 22
5. Bronstein AM, Bronstein MM, Kimmel R (2006) Generalized multidimensional scaling: a framework for isometry-invariant partial surface matching. Proc Natl Acad Sci (PNAS) 103(5):1168–1172
6. Bronstein AM, Bronstein MM, Kimmel R, Mahmoudi M, Sapiro G (2009) A Gromov-Hausdorff framework with diffusion geometry for topologically-robust non-rigid shape matching. Int J Comput Vis (IJCV) 89(2–3):266–286

7. Chui H, Rangarajan A (2003) A new point matching algorithm for non-rigid registration. Comput Vis Image Underst 89:114–141
8. Clarkson KL, Woodruff PD (2013) Low rank approximation and regression in input sparsity time. In Proceedings of the 45th Annual ACM Symposium on Symposium on Theory of Computing, STOC '13, pages 81–90, New York, NY, USA. ACM
9. Cohen MB, Peng R (2014) ℓp Row Sampling by Lewis Weights. CoRR abs/1412.0588
10. Cohen MB, Lee YT, Musco C, Musco C, Peng R, Sidford A (2014) Uniform sampling for matrix approximation. CoRR, abs/1408:5099
11. Cohen-Or D, Wolf L, Hamarneh G (2011) Prior Knowledge for Part Correspondence. Computer Graphics Forum, 553–562
12. Dasgupta A, Drineas P, Mahoney MW, Muthukrishnan S (2006) Sampling algorithms for l2 regression and applications. In Proceedings of the seventeenth annual ACM-SIAM symposium on Discrete algorithm, SODA '06, pages 1127–1136, New York. ACM
13. Drineas P, Malik M-I, Mahoney MW, Woodruff PD (2012) Fast approximation of matrix coherence and statistical leverage. ICML
14. Dubrovina A, Kimmel R (2010) Matching shapes by eigendecomposition of the Laplace-Beltrami operator. In: International Symposium on 3D Data Processing Visualization and Transmission (3DPVT)
15. Dunbar D, Humphreys G (2006) A spatial data structure for fast Poisson-disk sample generation. ACM Trans Graph (TOG) 25(3):503–508
16. Elad A, Kimmel R (2003) On bending invariant signatures for surfaces. IEEE Trans Pattern Anal Mach Intell (PAMI) 25(10):1285–1295
17. Gal R, Cohen-Or D (2006) Salient geometric features for partial shape matching and similarity. ACM Trans Graph (1):130–150
18. Golovinskiy A, Funkhouser T (2009) Consistent segmentation of 3D models. Comput Graph 33(3):262–269
19. Hu J, Hua J (2009) Salient spectral geometric features for shape matching and retrieval. Vis Comput 25(5–7):667–675
20. Jain, V., Zhang, H., Van Kaick, O.: Non-rigid spectral correspondence of triangle meshes. Int J Shape Model 13(1), 101–124 (2007)
21. Kim V, Lipman Y, Chen X, Funkhouser T (2010) Mobius transformations for global intrinsic symmetry analysis. In: Proceedings of the Eurographics Symposium on Geometry Processing (SGP). Wiley Online Library
22. Lei HP, Luo X-N, Lin S-J, Sheng J-Q (2013) Automatic 3D shape co-segmentation using spectral graph method. J Comput Sci Technol 28(05):919–929
23. Lewis D (1978) Finite dimensional subspaces of lp. Stud Math 63(2):207–212
24. Lipman Y, Chen X, Daubechies I, Funkhouser T (2010) Symmetry factored embedding and distance. In ACM Transactions on Graphics (Proc. SIGGRAPH) 29(4), 103
25. Liu, R. Zhang, H. Shamir,A. Cohen-Or, D.: A part-aware surface metric for shape analysis. Comput Graph Forum 28, 2 (2009), 397–406
26. Mateus D, Horaud RP, Knossow D, Cuzzolin F, Boyer E (2008) Articulated shape matching using Laplacian eigenfunctions and unsupervised point registration. In: Proceedings of the IEEE Conference on Computer Vision and Pattern Recognition (CVPR)
27. Memoli F (2009) Spectral Gromov-Wasserstein distances for shape matching. In: Workshop on Non-Rigid Shape Analysis and Deformable Image Alignment (ICCV workshop, NORDIA'09),Kyoto, Japan
28. Mémoli F, Sapiro GG (2005) A theoretical and computational framework for isometry invariant recognition of point cloud data. Found Comput Math 5(3):313–347
29. Ovsjanikov M, Sun J, Guibas L (2008) Global intrinsic symmetries of shapes. Comput Graph Forum 27(5): 1341–1348
30. Raviv D, Bronstein AM, Bronstein MM, Kimmel R (2010) Full and partial symmetries of non-rigid shapes. Int J Comput Vis (IJCV) 89(1):18–39
31. Reuter M (2010) Hierarchical shape segmentation and registration via topological features of Laplace-Beltrami eigenfunctions. Int J Comput Vis 89(2):287–308
32. Reuter M, Wolter F-E, Peinecke N (2009) Laplace-Beltrami spectra as "shape-DNA" of surface and solids. Comput Aided Design 38(4):342–366
33. Rustamov RM (2007) Laplace-Beltrami eigenfunctions for deformation invariant shape representation. In Proceedings of SGP, pp. 225–233 Eurographics Association, Aire-la-Ville
34. Sahilliolu Y, Yemez Y (2013) Coarse-to-fine isometric shape correspondence by tracking symmetric flips. Comput Graph Forum 32(1):177–189
35. Shalom S, Shapira L, Shamir A, Cohen-Or D (2008) Part analogies in sets of objects

36. Shapira, L. Shamir, A. Cohen-Or, D. (2008) Consistent mesh partitioning and skeletonisation using the shape diameter function. Vis Comput, 24, 4
37. Sharma A, Horaud RP (2010) Shape matching based on diffusion embedding and on mutual isometric consistency. In: Proceedings of the Workshop on Nonrigid Shape Analysis and Deformable Image Alignment (NORDIA)
38. Sumner RW, Popovic J (2004) Deformation transfer for triangle meshes. In ACM Transactions on Graphics (Proc. SIGGRAPH), 399–405
39. Tevs A, Bokeloh M, Wand M, Schilling A, Seidel H-P (2009) Isometric registration of ambiguous and partial data. In: Proceedings of the IEEE Conference on Computer Vision and Pattern Recognition (CVPR) pp. 1185–1192
40. Thorstensen N, Keriven R (2009) Non-rigid shape matching using geometry and photometry. In: Asian Conference on Computer Vision, pp. 1–12. Springer
41. Van Kaick O, Zhang H, Hamarneh G (2011) Cohen-or, D.: a survey on shape correspondence. Comput Graph Forum 30(6):1681–1707
42. Van Kaick O, Tagliasacchi A, Sidi O, Zhang H, Cohen-Or D, Wolf L, Hamarneh G (2011) Prior knowledge for part correspondence. Comput Graph Forum (Proc EUROGRAPHICS) 30:2
43. Wang YH, Asafi S, Kaick O, Zhang H, Cohen-Or D, Chen BQ (2012) Active co-Analysis of a set of shapes. ACM Trans. on Graphics (Proc. SIGGRAPH Asia) 31(6):157:1–157
44. Yonathan A, Haim B, Ron K (2015a) On the optimality of shape and data representation in the spectral domain. SIAM J Imaging Sci 8(2):1141–1160
45. Yonathan A, Anastasia D, Ron K (2016) Spectral generalized multi-dimensional scaling. Int J Comput Vis 118(3):380–392
46. Yoshiyasu Y, Yoshida E (2016) Symmetry aware embedding for shape correspondence [J]. Comput Graph 60:9–22
47. Yoshiyasu Y, Yoshida E, Yokoi K, Sagawa R (2014) Symmetry-aware non rigid matching of incomplete 3D surfaces. In: Proceedings of computer vision and pattern recognition (CVPR)
48. Zaharescu A, Boyer E, Varanasi K, Horaud RP (2009) Surface feature detection and description with applications to mesh matching. In: Proceedings of the IEEE Conference on Computer Vision and Pattern Recognition (CVPR)
49. Zhang H, Sheffer A, Cohen-Or D, Zhou Q, van Kaick O, Tagliasacchi A (2008) Deformation-driven shape correspondence. Comput Graph Forum (Proc SGP) 27(5):1431–1439
50. Zigelman G, Kimmel R, Kiryati N (2002) Texture mapping using surface flattening via multidimensional scaling. IEEE Trans Vis Comput Graph 8(2):198–207

Han Li , female, bore in 1973. She is a distinguished professor in Liaoning Normal University. In 2007 she achieved doctoral degree from the school of Telecommunication and Information Technology in Trento University in Italy. And she carried out research work of the key European project (AIM@SHAPE) in Grenoble University in France as a visitor during that time. From 2008 to 2010 she worked in Academy of mathematics and systems science, Chinese academy of sciences as a postdoctoral researcher. She mainly engaged in computer graphics, computer vision and digital geometry processing fields. Recently, she has published more than 50 influential papers in International Journals and Chinese Journals. And she has won the Xu Guozhi postdoctoral reward of Chinese academy of science, the title of the selected person of Liaoning Provincial Million Talented

Person Project and a Thousand Talented person, excellent IT teacher reward in Dalian, Liaoning province natural science academic achievements and etc. So far, she has presided over the project supported by National Natural Science Foundation (NSF) of China, the project of Scientific Research Foundation for the Returned Overseas Chinese Scholars, State Education Ministry, the projects supported by Program for Liaoning Excellent Talents in University (LNET) and the projects funded by Liaoning Province Education Administration and so on. She has participated in two National 973 projects and two important European projects (AIM@SHAPE and IMPROVE). Currently, she is the member of China Computer Federation (CCF), and she is the evaluation experts of the State Education Ministry and the National Natural Science Foundation and reviewer of number of international and domestic Journals.